An Efficient Scattered-Field Formulation for Objects in Layered Media Using the FVTD Method

Dustin Isleifson, *Student Member, IEEE*, Ian Jeffrey, *Member, IEEE*, Lotfollah Shafai, *Life Fellow, IEEE*, Joe Lovetri, *Senior Member, IEEE*, and David G. Barber

***Abstract*—A technique for efficiently simulating the scattering from objects in multilayered media is presented. The efficiency of the formulation comes from the fact that the sources for the scattered fields (SFs) only occur at the inhomogeneities and, therefore, the SFs impinging on the boundaries are more easily absorbed. To demonstrate the technique, a 1-D-finite-difference time-domain solution to the plane-wave propagation through a multilayered medium is used as an incident-field source for an SF formulation of the finite-volume time-domain method. Practical aspects of the application are discussed and numerical examples for scattering from canonical objects are presented to show the validity of the proposed technique. The simulation scheme described herein can be used for simulations of geophysical media with appropriate specifications of the dielectric properties of the media and the inhomogeneities.**

***Index Terms*—Finite difference time domain (FDTD), finite volume time domain (FVTD), numerical methods.**

I. Introduction

THE STUDY of electromagnetic wave scattering from objects in multilayered media is a widespread problem with diverse applications including the remote sensing of earth environments [1] and buried object detection [2], [3]. In contrast to the problem where the target or object of interest lies in free space, the formulation and subsequent analysis of the multilayered media are complicated due to the layer interfaces that govern the propagation of the interrogating incident field. Determining a simple way to account for the layers is a nontrivial task, which has led to a variety of techniques in the literature for modeling subsurface problems [4] (and references therein) [5]. As stated in [6], a variety of analytic methods has been developed and is capable of describing the propagation through multilayered media; however, it is challenging to utilize these methods in an existing numerical solver.

Differential-equation-based techniques are particularly well suited for modeling wave interactions with inhomogeneities in a multilayered medium since the incorporation of an inhomogeneity does not increase the number of unknowns that must be solved [6]. The ubiquitous finite-difference time-domain (FDTD) method [7] has been used in this respect, and while it is appropriate for many geometries, it is deficient in that it requires a high level of discretization in order to resolve objects with curved features. In many subsurface scattering problems, the inhomogeneities exhibit curved features (e.g., brine inclusions in sea ice, landmines, cancerous tumors) and so, a method that takes the curved features into account would be useful. One such method is the finite-volume time-domain (FVTD) method [8], [9], which is particularly well suited to modeling curved features due to its ability to use a conforming irregular grid. With appropriate interpolation methods, the solutions for the multilayered problem that have been developed for the FDTD method can be used with the FVTD method.

When using a scattered-field (SF) technique to perform calculations, knowledge of the incident field at the inhomogeneity for the entire time history of the simulation is required. When the medium is multilayered, the incident field at the inhomogeneity is the resultant of various reflections from and transmissions across the layer interfaces. The SFs generated by the inhomogeneity then propagate in the multilayered medium and are absorbed at the boundaries. In time-domain differential-equation-based methods, the boundary conditions are more efficient at absorbing normally incident SFs, and so, the incorporation of the incident field into the numerical method and solving for only the SF allows the boundary condition to be more effective.

A method for generating a total-field/SF (TF/SF) source for general layered media was presented in [10]. Continued interest in developing the technique is evident in the variations that have been presented in the literature (for example, [11] and [12]). Previously, [6] presented an FDTD method for modeling scatterers in stratified media, but they limited their study to time-harmonic plane waves. In this paper, we adapt the general TF/SF source for use in an SF formulation of the FVTD method and show how it can be used for scattering from objects within a multilayered medium. The focus of [10] is mostly on computational aspects, such as stability, dispersion, and evanscent waves; their examples are strictly multilayered media without any inhomogeneities. In contrast, our work focuses on the utilization of the method for providing an incident field and calculating the scattering from inhomogeneities lying within the medium. Furthermore, our work considers an interpolation scheme that permits an irregular mesh, such as that utilized in the FVTD calculation. To validate our method, we compare with other published data for canonical shapes lying within a half-space medium and below a lossy layer. Incorporation of the SF formulation for

Manuscript received October 27, 2010; revised March 01, 2011; accepted April 23, 2011. Date of publication August 12, 2011; date of current version November 02, 2011. This work was supported by an NSERC graduate scholarship to the first author, and NSERC operating grants and a Canada Research Chairs grant to the third author.

D. Isleifson, I. Jeffrey, L. Shafai, and J. LoVetri are with the Department of Electrical and Computer Engineering, University of Manitoba, Winnipeg, MB R3T 2N2, Canada (e-mail: shafai@ee.umanitoba.ca; joe_lovetri@umanitoba.ca; disleifson@gmail.com; ijeffrey@ee.umanitoba.ca).

D. G. Barber is with the Centre for Earth Observation Science and the Faculty of Environment, University of Manitoba, Winnipeg, MB R3T 2N2, Canada (e-mail: dbarber@cc.umanitoba.ca).

Digital Object Identifier 10.1109/TAP.2011.2164198

multilayered media in the FVTD engine provides a new tool for modeling complex layered media and has future potential to be used for modeling electromagnetic interactions in remote sensing studies.

The organization of this paper is as follows. In Section II. we formulate the total-field/SF background theory. Details of the practical application of this general concept in an FVTD numerical solver are given in Section III. We present numerical results for several canonical shapes for validation in Section IV. We conclude with several remarks on the implementation and applicability of the method, along with some suggestions for our future work.

II. Formulation

Let us denote the time-domain electric-field intensity as $\mathbf{E}(\mathbf{r},t)$, the time-domain magnetic-field intensity as $\mathbf{H}(\mathbf{r},t)$, the relative permittivity as $\epsilon(r)$, the relative permeability as $\mu(r)$, and the impressed time-domain electric current as $\mathbf{J}(\mathbf{r},t)$. Using the standard incident-field-SF decomposition, we have

$$\mathbf{E}(\mathbf{r},t) \triangleq \mathbf{E}^{\text{inc}}(\mathbf{r},t) + \mathbf{E}^{sc}(\mathbf{r},t) \tag{1}$$

and

$$\mathbf{H}(\mathbf{r},t) \triangleq \mathbf{H}^{\text{inc}}(\mathbf{r},t) + \mathbf{H}^{sc}(\mathbf{r},t) \tag{2}$$

where the incident fields are defined to exist in a background media, with $\epsilon_b(r)$ and $\mu_b(r)$, and are produced by the impressed current $\mathbf{J}(\mathbf{r},t)$. That is

$$\nabla \times \mathbf{E}^{\text{inc}}(\mathbf{r},t) = -\mu_b(\mathbf{r})\frac{\partial \mathbf{H}^{inc}(\mathbf{r},t)}{\partial t} \tag{3}$$

$$\nabla \times \mathbf{H}^{\text{inc}}(\mathbf{r},t) = \epsilon_b(\mathbf{r})\frac{\partial \mathbf{E}^{\text{inc}}(\mathbf{r},t)}{\partial t} + \mathbf{J}(\mathbf{r},t). \tag{4}$$

The SF is then produced by the difference between the true media $\epsilon(\mathbf{r})$ and $\mu(\mathbf{r})$, and the background. After some algebraic manipulation

$$\nabla \times \mathbf{E}^{sc}(\mathbf{r},t) = -\mu(\mathbf{r})\frac{\partial \mathbf{H}^{sc}(\mathbf{r},t)}{\partial t} - \mathbf{M}_c(\mathbf{r},t) \tag{5}$$

$$\nabla \times \mathbf{H}^{sc}(\mathbf{r},t) = \epsilon(\mathbf{r})\frac{\partial \mathbf{E}^{sc}(\mathbf{r},t)}{\partial t} + \mathbf{J}_c(\mathbf{r},t) \tag{6}$$

where the contrast magnetic and electric contrast sources are defined as

$$\mathbf{M}_c(\mathbf{r},t) = [\mu(\mathbf{r}) - \mu_b(\mathbf{r})]\frac{\partial \mathbf{H}^{\text{inc}}(\mathbf{r},t)}{\partial t} \tag{7}$$

$$\mathbf{J}_c(\mathbf{r},t) = [\epsilon(\mathbf{r}) - \epsilon_b(\mathbf{r})]\frac{\partial \mathbf{E}^{\text{inc}}(\mathbf{r},t)}{\partial t}. \tag{8}$$

For nonmagnetic media, $\mathbf{M}_c(\mathbf{r},t) = 0$. If we take the incident field to propagate in the layered background medium with no inhomogeneities, then it is clear from (8) that the SF is generated by equivalent sources at the inhomogeneities. The fact that the sources for the SF occur only at the inhomogeneities means that the field impinging on the boundaries is more easily absorbed by whatever absorbing boundary condition is being used. The incident field still contains all of the information on the interactions of the waves as they propagate from one layer to another and scatter from the layer interfaces. One of the benefits of using the SF formulation is that the incident-field can be specified either analytically or numerically.

III. Numerical Implementation

In order to demonstrate the utility of the SF formulation as a general concept, we apply the method into the framework of an existing FVTD numerical solver. This is similar to the approach used in [6], where a time-harmonic plane-wave source was applied to a scatterer in a finely stratified layered medium. In our work, we focus on the FVTD method for numerically solving Maxwell's equations and utilize a numerically defined (as opposed to an analytically defined) incident-field source term. A technique similar to the one presented here can be used with any time-domain field solver.

A. FVTD Computations

The FVTD method is a robust and flexible scheme for numerically simulating 3-D electromagnetic problems [8], [9]. It is an $O(N)$ solver, which means that it scales linearly with the number of elements in the mesh. One of the advantages FVTD has over the FDTD algorithm is that structured and arbitrary unstructured meshes are equally suitable discretizations for FVTD simulations. This implies that the volumetric mesh can be created to naturally follow oblique surfaces and no alteration to the algorithm is required to compensate for an inaccurate physical model.

The FVTD formulation used for the numerical simulations produced in this work is a cell-centered, upwind, characteristic-based numerical engine for meshes consisting of first-order polyhedral elements [9]. It is second order accurate in time and space. The engine is capable of solving Maxwell's equations in the time domain using either a total- or SF formulation, the latter permitting arbitrary (i.e., nonhomogeneous) background media [13]. The numerical implementation has been parallelized for distributed parallel environments by decomposing the computational domain into subdomains by using orthogonal-recursive bisection (ORB). Each subdomain is assigned to a unique processor and the underlying system of partial differential equations is solved locally on each processor by introducing a halo/ghost duplication of elements lying on the boundary of a processor's domain [9].

The upwind formulation explicitly imposes the electromagnetic boundary conditions at the facets of each mesh element. Not only does this achieve accurate modeling of irregularly shaped inhomogeneous objects, but also allows for very simple, but effective absorbing boundary conditions (ABC) at the edges of the computational domain without having to introduce perfectly matched layers (PML). These ABCs are known as the Silver–Müller conditions. PML absorbing boundary conditions have also been implemented [14]. Due to its advantages, FVTD is an excellent candidate for solving field problems with a large number of small inhomogeneities.

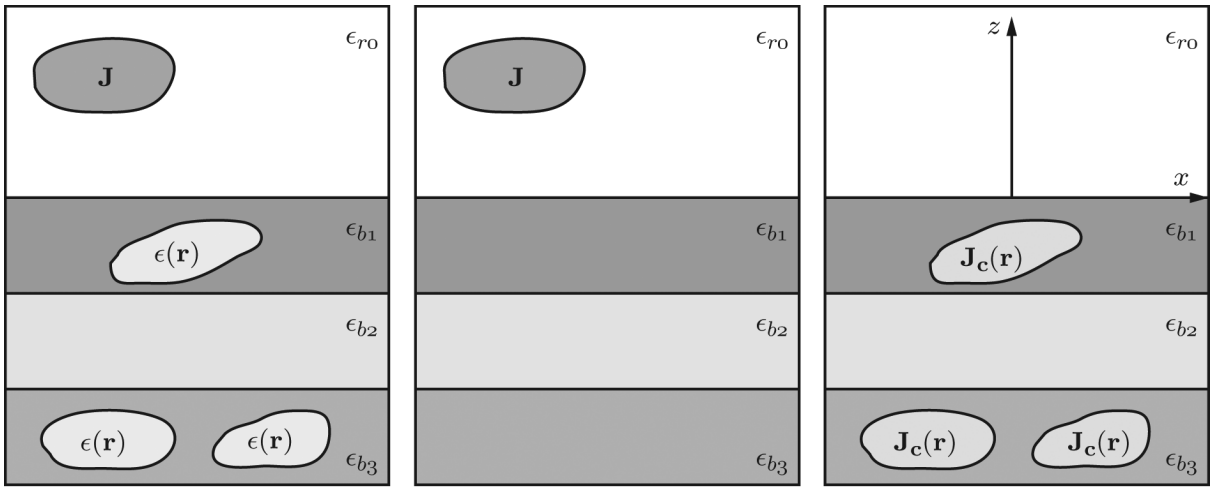

Fig. 1. Hypothetical geometry illustrating the decomposition of the fields in the SF formulation. (a) Total-field geometry. (b) Incident-field geometry. (c) SF geometry.

B. Plane-Wave Injector

When simulating multilayered media, truncating a plane wave in a total-field formulation is very inefficient because the incident-wave vector is impinging tangentially (or close to tangentially) to the ABC. This is the worst possible case for the ABC to absorb the wave. In addition, spurious reflections occur where the layer interfaces meet the boundary conditions, corrupting the desired SFs from objects within the layered medium. In effect, it is impossible to distinguish between SFs from the objects and erroneous SFs from the ABC.

One way to mitigate this problem is through the use of the SF formulation. A total-field simulation can be performed to obtain the total fields for a wave propagating in layered media. We then use this total field as the incident field in an SF formulation. A hypothetical SF decomposition is shown in Fig. 1 for the case of multilayered media. Following [10], we utilize a 1-D-FDTD solution for a wave propagating through layered media at an arbitrary incidence angle, with appropriate modifications for the FVTD method. For completeness, the derived expressions for TE and TM wave propagation are summarized here.

The TE equations for plane-wave propagation through multilayered media are given as

$$\frac{\partial E_y}{\partial z} = \mu_0 \frac{\partial H_x}{\partial t}, \tag{9}$$

$$\frac{\partial H_x}{\partial z} = \epsilon_0(\epsilon_r - \epsilon_{r0} sin^2\theta)\frac{\partial E_y}{\partial t} \tag{10}$$

$$H_z = Y_0\sqrt{\epsilon_{r0}} sin\theta E_y \tag{11}$$

where θ is the incidence angle measured between the direction of propagation and the z axis, $Y_0 = \sqrt{\epsilon_0/\mu_0}$ is the intrinsic admittance of free space, and ϵ_{r0} is the dielectric constant of the uppermost (or 0th) layer.

Similarly, the TM equations are given as

$$\frac{\partial E_x}{\partial z} = -\mu_0 \frac{\partial H_y}{\partial t}\frac{(\epsilon_r - \epsilon_{r0} sin^2\theta)}{\epsilon_r} \tag{12}$$

$$\frac{\partial H_y}{\partial z} = -\epsilon_0\epsilon_r \frac{\partial E_x}{\partial t} \tag{13}$$

$$E_z = \frac{Z_0\sqrt{\epsilon_{r0}} sin\theta}{\epsilon_r} E_y \tag{14}$$

where $Z_0 = \sqrt{\mu_0/\epsilon_0}$ is the intrinsic impedance of free space.

These equations resemble the familiar transmission-line equations and with appropriate descriptions of the dielectric profile in the z-direction, they describe the propagation of a plane wave through layered media. In order to include lossy material, a variation to the TM equations must be made (not demonstrated in this paper, but described in [10]). To solve the TE or TM equations, we discretize the equations, following the approach of [15], where the electric- and magnetic-field components are interleaved, and we use a central-difference approximation. We set the temporal discretization to obey the Courant stability criterion $\Delta t \leq \Delta z/v_0$, where v_0 is the velocity of propagation in the layer with the lowest dielectric constant. We apply a basic PML boundary condition at the upper and lower bounds of the 1-D solution grid, but also pad the solution domain to minimize the error created by the boundary (i.e., add more distance for the wave to travel than is necessary for the FVTD solution). This has no impact on the memory required to store the 1-D solution since we only keep the portion which will correspond to the variation required within the FVTD domain, but it does remove artificial reflections created from the boundaries in the 1-D solution.

In practice, the 1-D solution is interpolated into the 3-D irregular mesh that is used in the FVTD computations. A principle plane containing the time history of the plane-wave propagation through layered media is made to coincide with the xz plane. To find the field values along this principle plane, we need only a time shift, since this is a property of plane-wave propagation. This concept is illustrated in Fig. 2, where the principle plane is shown to coincide with the xz plane, and $\tau = x_1 \sin(\theta)/c_0$ (c_0 is the speed of light in a vacuum). The solution for wave propagation along the negative z axis is calculated and the time-delayed result is utilized to find the field value at a location x_1.

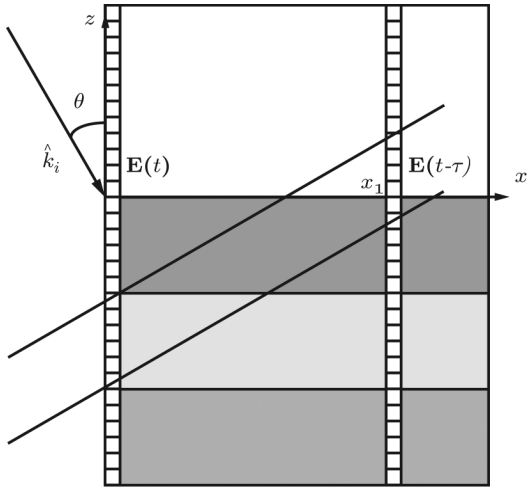

Fig. 2. Calculation of field values on the principle plane using the time-delay factor τ. The fields calculated at x_1 are the fields calculated along the z axis with an appropriate time delay.

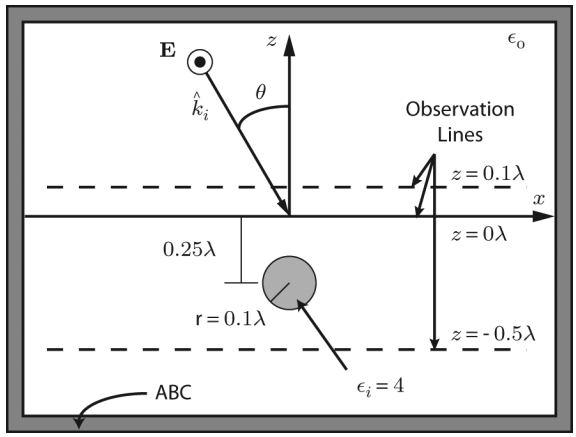

Fig. 3. Geometry for a dielectric sphere in free space, with a radius of 0.1 λ, and centered at $z = -0.25\lambda$.

To obtain a 3-D representation, we utilize the invariance of the solution along the other coordinate axis (y axis).

C. Interpolation of the 1-D FDTD Solution to the FVTD Grid

Many practical implementation issues exist, such as choosing an appropriate interpolation method and ensuring that the spatial discretization of the auxiliary 1D-FDTD simulation does not cause dispersion in the main FVTD simulation. If the FVTD grid were regular (as would be used in a 3-D-FDTD grid), we could follow the method of [10] and increase the spatial sampling by an odd factor and thereby ensure that the interfaces were preserved. Moreover, since the auxiliary FDTD simulation takes a small fraction of the time needed for the overall FVTD scattering simulation, we choose the spatial discretization to be much smaller than that of the overall FVTD mesh. Cubic spline spatial interpolations and nearest-neighbor temporal interpolations are performed to find the corresponding field values in the centroids of the $3D$ elements (tetrahedrons) that make up the FVTD mesh.

The results of the incident-field propagation are calculated and stored in arrays in memory. They are potentially accessed only during the update scheme of the FVTD simulations, which checks to see whether the contrast between the background mesh (that which is seen by the incident field) and the scattered field mesh are nonzero. When they are nonzero, this indicates the presence of a contrast source (i.e., $\mathbf{J}_c(\mathbf{r}, t) \neq 0$) and a scattered field is generated at that particular mesh element. This means that results of the incident-field interpolations are only used when needed and they are not calculated and stored throughout the entire mesh, which would be inefficient.

IV. Numerical Results and Discussion

In this section, we calculate the scattered near-field values for a variety of objects located within a planarly layered medium. Canonical examples are chosen so that comparisons can be made with other published data in the literature. We have found that there is a dearth of examples that compute and provide graphical results for the near-field scattering from objects within multilayered media, despite the fact that this problem is conceptually well known. In particular, we provide comparisons with the work in [5] (which provides a method based on the Born approximation) and [16] (which introduced a method based on the method of moments).

The computational geometry was created by using a freeware mesh-generating program GMSH [17], which was also used to transform the physical description into a mesh for FVTD computations. The time function of the input waveform was a Gaussian derivative

$$E_y(t) = \frac{2A(t-t_0)}{b^2} \exp\left(\frac{-(t-t_0)^2}{b^2}\right) \tag{15}$$

where $A = 1$, $t_0 = 0.2$ ns, and $b = 70$ ps. The constants in (15) were chosen so that sufficient energy would propagate at the frequency of interest (specifically 6 GHz).

A. Scattering From a Dielectric Sphere

For our first example, we consider a dielectric sphere in a free-space background. In this case, we are able to compare our results with the commercially available software program FEKO. The permittivity value of the sphere is set to $\epsilon_i = 4$, and the radius of the sphere is 0.1 λ. The geometry of the problem (for FVTD) is given in Fig. 3, with the sphere centered at $z = -0.25\lambda$. The results of our computations using FVTD and FEKO at $z = -0.5\lambda$, $z = 0\lambda$, and $z = 0.01\lambda$ are given in Fig. 4. The excellent agreement between the results shows the validity of the scheme.

B. Scattering From a Dielectric Cube

For our next example, we consider a dielectric cube buried in a half-space medium. Both the half-space and the dielectric cube are lossy, with permittivity values of $\epsilon_b = 3 - j0.1$ and $\epsilon_i = 2.9 - j0.05$. To calculate the conductivity that must be used in the FVTD simulations, we used a frequency of 6 GHz, which gives conductivities as $\sigma_b = 0.03338$ [S/m] and $\sigma_i = 0.01669$ [S/m]. Our results are normalized to the free-space wavelength, as in [5]. The geometry of the problem is given in Fig. 5, and the results of our computations at $z = 0.1\lambda$ are given in Fig. 6. In comparison with [5], our results are slightly higher; however, in comparison with [16], our results are very similar. For example,

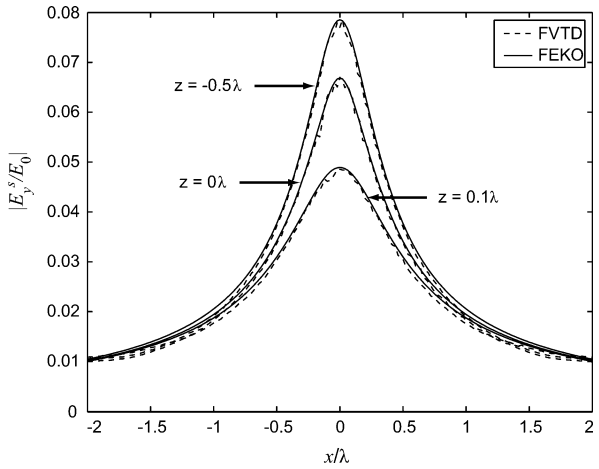

Fig. 4. Scattered electric fields for a dielectric sphere in free space, centered at $z = -0.25\lambda$. FVTD results are compared with FEKO.

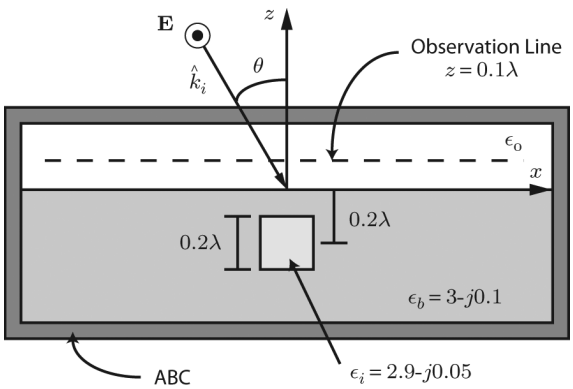

Fig. 5. Geometry for a lossy dielectric cube buried in a lossy half-space.

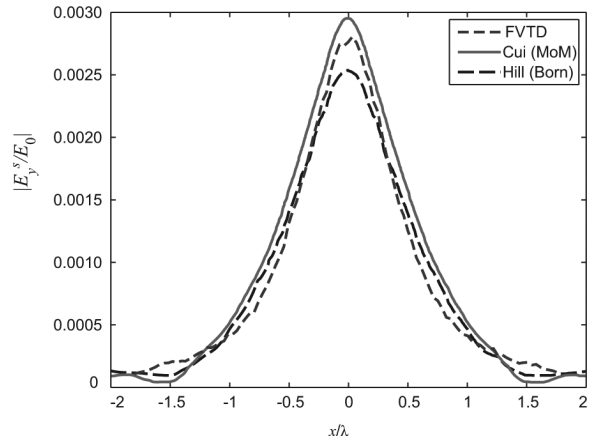

Fig. 6. Scattered electric fields for a lossy dielectric cube buried in a lossy half-space at $z = 0.1\lambda$. FVTD results are compared with [16] (Cui, MoM) and [5] (Hill, Born Approximation).

our peak value at $z = 0.2\lambda$ is 0.002, while [5] reports 0.0017 and [16] reports 0.002. The difference is associated with the error in using the Born approximation [16]. The decay of the curve appears to be in agreement as well.

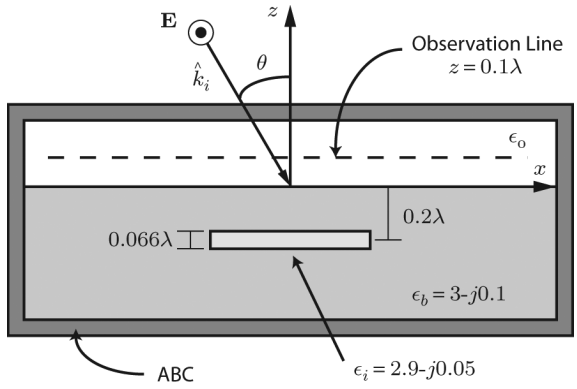

Fig. 7. Geometry for a lossy dielectric box buried in a lossy half-space. The box dimensions are 0.6 λ, 0.2 λ and 0.066 λ for the x, y, and z dimensions, respectively.

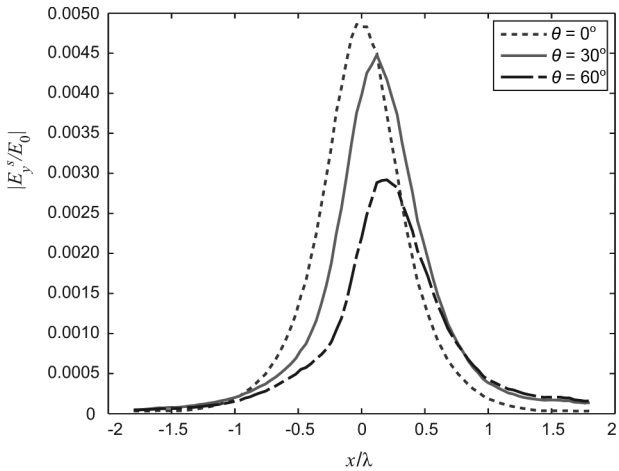

Fig. 8. Scattered electric fields for various incidence angles for a lossy dielectric box buried in a lossy half-space.

C. Scattering From a Dielectric Box

To show the variation of the scattered electric fields as a function of incidence angle, we consider another one of the examples presented in [5]. In this case, the buried object is a rectangular box, with a size given by 0.6 λ, 0.2λ, and 0.066 λ for the x, y, and z dimensions, respectively. The geometry of the problem is given in Fig. 7, and the results of our computations are given in Fig. 8. For $\theta_i \neq 0°$, the peak of the scattered field has shifted toward the specular direction, and the magnitude of the peak decreases as the incidence angle increases. This is similar to the result observed in [5], although our magnitudes are slightly different because those in [5] are obtained by using an approximate technique.

D. Scattering From a Dielectric Slab in a Half-Space

The previous examples considered were weak scatterers (i.e., the dielectric contrast is not very large). For this example, we consider a stronger scatterer, following the examples in [16]. Both the half-space and the dielectric slab are lossy, with permittivity values of $\epsilon_b = 4 - j0.5$ and $\epsilon_i = 10 - j5$. At the frequency of 6 GHz, the conductivities are $\sigma_b = 0.16689$ [S/m] and $\sigma_i = 1.6689$ [S/m]. The geometry of the problem is given in

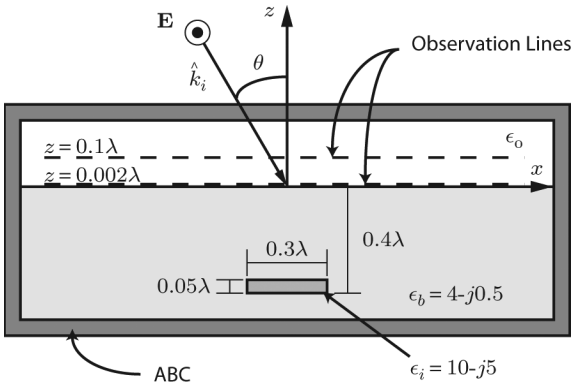

Fig. 9. Geometry for a lossy dielectric slab buried in a lossy half-space. Slab dimensions are 0.3 λ, 0.3 λ, and 0.05 λ for the x, y, and z dimensions, respectively.

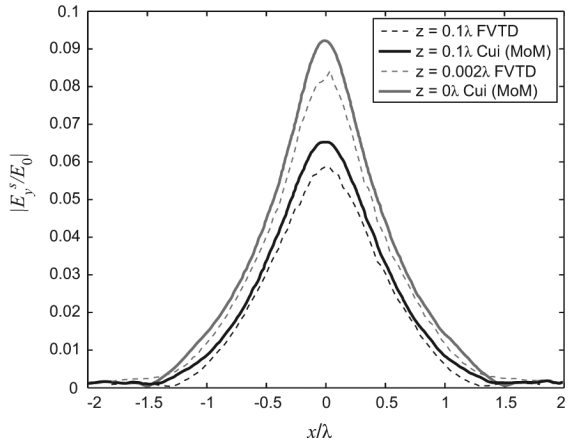

Fig. 10. Scattered electric fields for a lossy dielectric slab buried in a lossy half-space. FVTD results are compared with [16] (Cui, MoM).

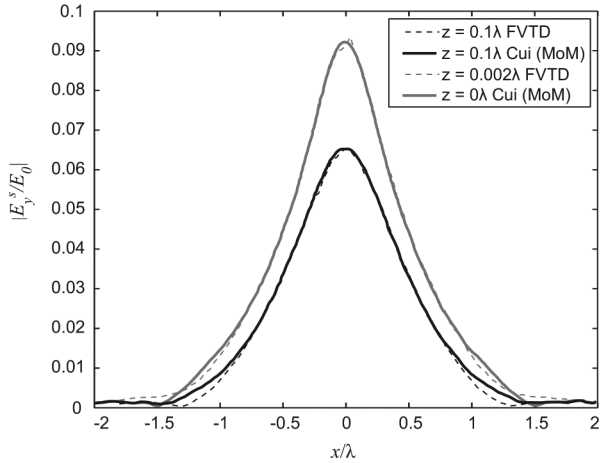

Fig. 11. Scattered electric fields for a lossy dielectric slab buried in a lossy half-space. FVTD results are normalized to [16] (Cui, MoM).

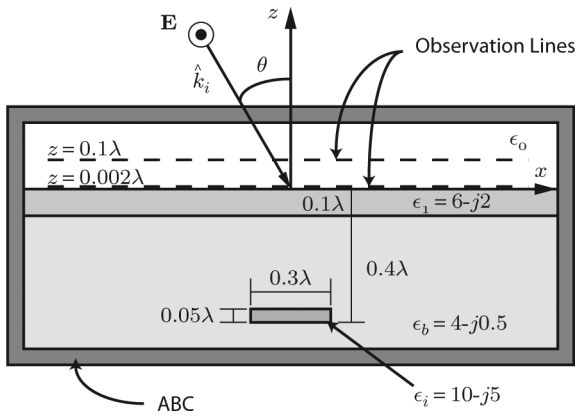

Fig. 12. Geometry for a lossy dielectric slab buried in a lossy half-space beneath another lossy layer. Slab dimensions are 0.3 λ, 0.3 λ, and 0.05 λ for the x, y, and z dimensions, respectively.

Fig. 9, and the results of our computations are given in Fig. 10. In comparison with [16], our results are similar, but slightly lower, similar to the example of the dielectric cube. For example, our peak value at $z = 0.002\lambda$ is 0.081, while [16] reports 0.092 at $z = 0$, yielding a relative error of about 12%. As another example, our peak value at $z = 0.01\lambda$ is 0.0599, while [16] reports 0.066 at $z = 0.01\lambda$, yielding a relative error of about 9%. We consider this relative error to be acceptable considering the differences in the computational methods. As an additional test, we rescaled our simulation results to the peak value of the result at $z = 0$, and these results are presented in Fig. 11. It is clear that our results match up extremely well with those of [16] as long the as they are normalized.

E. Scattering From a Dielectric Slab in Multilayered Media

As a modification to the dielectric slab example, we consider the same slab buried under a lossy dielectric layer. Again, the half-space and the dielectric slab are lossy, with permittivity values of $\epsilon_b = 4 - j0.5$ and $\epsilon_i = 10 - j5$, with the lossy layer of $\epsilon_1 = 6 - j2$. The conductivity of the lossy layer is $\sigma_1 = 0.66756$ [S/m]. The geometry of the problem is given in Fig. 12, and the results of our computations are given in Fig. 13. In comparison with [16], our results are very similar. For example, our peak value at $z = 0.002\lambda$ is 0.0387, while the corresponding peak value reported in [16] is 0.042, yielding a relative error of about 8%. As another example, our peak value at $z = 0.01\lambda$ is 0.0283, while [16] reports 0.031 corresponding to the same height above the surface, yielding a relative error of about 9%. We consider this to be acceptable considering the differences in the computational methods. Again, as an additional test, we rescaled our simulation results to the peak value of the result at $z = 0$, and these results are presented in Fig. 14. This scale factor was the same value as in the previous example (slab in a half-space). It is clear that our results match up extremely well with those of [16] as long as they are normalized. Since the slab buried in a half-space and the slab buried in a multilayered medium had the same scale factor, we hypothesize that this is a constant difference between the two methods. The exact nature of the difference cannot be determined at this point; however, we are confident that our methodology is sound due to our accurate comparison with the sphere in free space using FEKO.

F. Scattering From Dielectric Spheres

In most of our previous examples, we used shapes with a cubic geometry, yet in our introduction, we suggested that one of

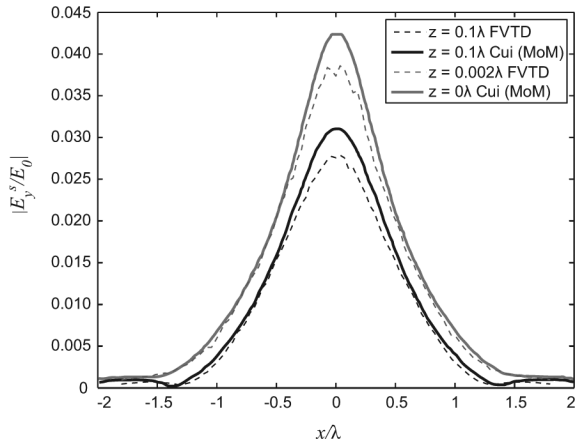

Fig. 13. Scattered electric fields for a lossy dielectric slab buried in a lossy multilayered medium. FVTD results are compared with [16] (Cui, MoM).

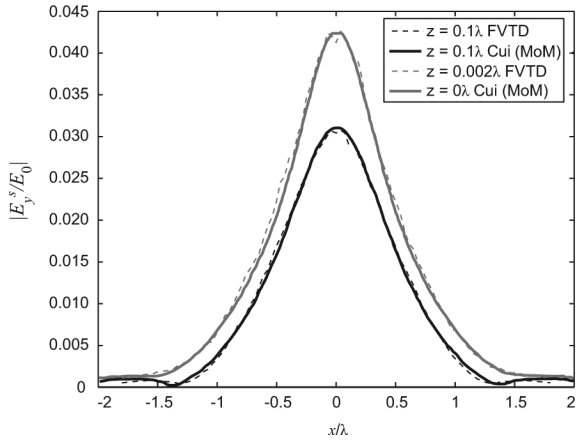

Fig. 14. Scattered electric fields for a lossy dielectric slab buried in a lossy multilayered medium. FVTD results are normalized to [16] (Cui, MoM).

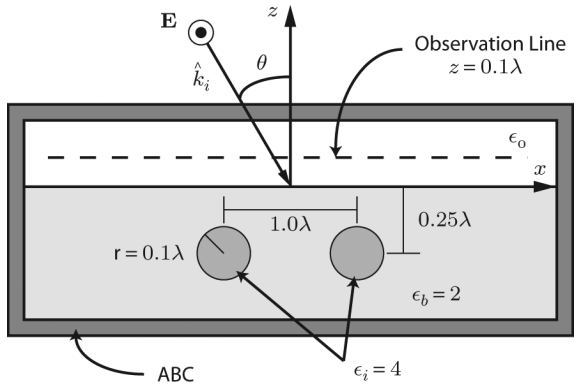

Fig. 15. Geometry for dielectric spheres buried in a half-space. Sphere radii are 0.1λ, separation is 1.0 λ, and sphere centers are $z = -0.25\lambda$.

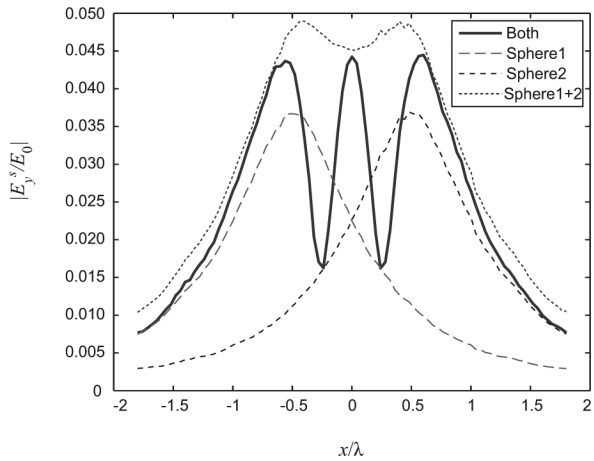

Fig. 16. Scattered electric fields for spheres buried in a half-space. Solid line: simultaneous scattering from both spheres, dotted line: superposition of sphere 1 and sphere 2 scattered fields.

the major benefits of using the FVTD method versus the FDTD method was the ability to have a mesh conform to an irregular surface. In this example, we present the scattering for multiple spheres buried in a dielectric half-space. This type of problem is very common in scattering simulations of geophysical media, where the subsurface can be populated with regions of dielectric discontinuity (for example, brine pockets in sea ice). The proximity of spheres is also an issue in studies involving the homogenization of random media [18]. The geometry of the computational domain for the case of two spheres is shown in Fig. 15. We simulated the scattering from both spheres simultaneously, from sphere 1 only (the left-hand sphere in Fig. 15), and from sphere 2 only (the right-hand sphere in Fig. 15). The simulation results are presented in Fig. 16, where we have also plotted the superposition of the scattering from sphere 1 and sphere 2. It is clear from the plotted results that multiple spheres must be simulated simultaneously since an attempt to approximate the scattering by superposition does not apply when the spheres are in close proximity. The importance of the proximity effect was also discussed in [19], particularly with regards to discrete modeling in remote sensing studies. Since our future work includes modeling electromagnetic scattering for remote sensing, it is important that we should examine and consider these effects before embarking on such modeling studies.

V. Conclusion

Through incorporating the SF formulation for multilayered media in an FVTD engine, an efficient method of modeling complex layered media has been developed. In this paper, we have presented details of the method used to calculate electromagnetic scattering from objects buried in multilayered media, which has a wide range of potential applications. Our method is capable of calculating the scattering from multiple objects with a minimal increase in the number of unknowns in the computation. Comparisons with other published data in the literature provided good agreement, giving us confidence in the FVTD implementation that we have developed. In our future research, we intend to use the proposed method for modeling electromagnetic scattering from geophysical media, with an application to remote sensing studies.

ACKNOWLEDGMENT

The authors would like to thank V. Okhmatovski for the use of his computing cluster.

REFERENCES

[1] S. V. Nghiem, R. Kwok, S. H. Yueh, and M. R. Drinkwater, "Polarimetric signatures of sea ice 1. theoretical model," *J. Geophys. Res.*, vol. 100, no. C7, 1995.

[2] M. El-Shenawee, "Polarimetric scattering from two-layered two-dimensional random rough surfaces with and without buried objects," *IEEE Trans. Geosci. Remote Sens.*, vol. 42, no. 1, pp. 67–76, Jan. 2004.

[3] C. D. Moss, F. L. Teixeira, Y. E. Yang, and J. A. Kong, "Finite-difference time-domain simulation of scattering from objects in continuous random media," *IEEE Trans. Geosci. Remote Sens.*, vol. 40, no. 1, pp. 178–186, Jan. 2002.

[4] T. J. Cui and W. C. Chew, "Fast evaluation of sommerfeld integrals for electromagnetic scattering and radiation by three-dimensional buried objects," *IEEE Trans. Geosci. Remote Sens.*, vol. 37, no. 2, pp. 887–900, Mar. 1999.

[5] D. Hill, "Electromagnetic scattering by buried objects of low contrast," *IEEE Trans. Geosci. Remote Sens.*, vol. 26, no. 2, pp. 195–203, Mar. 1988.

[6] K. Demarest, R. Plumb, and Z. Huang, "FDTD modeling of scatterers in stratified media," *IEEE Trans. Antennas Propag.*, vol. 43, no. 10, pp. 1164–1168, 1995.

[7] A. Taflove and S. C. Hagness, *Computational Electrodynamics: The Finite-Difference Time-Domain Method*, 2nd ed. Norwood, MA: Artech House, 2000.

[8] P. Bonnet, X. Ferrieres, P. L. Michielsen, and P. Klotz, *Finite Volume Time Domain Method*, S. M. Rao, Ed. San Diego, CA: Academic Press, 1999.

[9] D. Firsov, J. LoVetri, I. Jeffrey, V. Okhmatovski, C. Gilmore, and W. Chamma, "High-order FVTD on unstructured grids using an object-oriented computational engine," . *Proc. Appl. Comput. Electromagn. Soc.*, vol. 22, no. 1, pp. 71–82, 2007.

[10] I. Capoglu and G. Smith, "A total-field/scattered-field plane-wave source for the FDTD analysis of layered media," *IEEE Trans. Antennas Propag.*, vol. 56, no. 1, pp. 158–169, Jan. 2008.

[11] Y. Fang, L. Wu, and J. Zhang, "Excitation of plane waves for FDTD analysis of anisotropic layered media," *IEEE Antennas Wireless Propag. Lett.*, vol. 8, pp. 414–417, 2009.

[12] T. Tan and M. Potter, "FDTD discrete planewave (FDTD-DPW) formulation for a perfectly matched source inTFSF simulations," *IEEE Trans. Antennas Propag.*, vol. 58, no. 8, pp. 2641–2648, Aug. 2010.

[13] D. Isleifson, L. Shafai, J. LoVetri, and D. G. Barber, "On the development of a scattered-field formulation for objects in layered media using the FVTD method," presented at the Int. Rev. Progr. Appl. Comput. Electromagn. Symp., Williamsburg, VA, 2011.

[14] K. Sankaran, C. Fumeaux, and R. Vahldieck, "Cell-centered finite-volume-based perfectly matched layer for time-domain Maxwell system," *IEEE Trans. Microw. Theory Tech.*, vol. 54, no. 3, pp. 1269–1276, Mar. 2006.

[15] K. S. Yee, "Numerical solution of initial boundary value problems involving Maxwell's equations in isotropic media," *IEEE Trans. Antennas Propag.*, vol. 14, no. 3, pp. 302–307, May 1966.

[16] T. J. Cui, W. Wiesbeck, and A. Herschlein, "Electromagnetic scattering by multiple three-dimensional scatterers buried under multilayered media. II numerical implementations and results," *IEEE Trans. Geosci. Remote Sens.*, vol. 36, no. 2, pp. 535–546, Mar. 1998.

[17] C. Geuzaine and J.-F. Remacle, "Gmsh: A three-dimensional finite element mesh generator with built-in pre- and post-processing facilities," *Int. J. Num. Meth. Eng.*, vol. 79, no. 11, pp. 1309–1331, 2009.

[18] D. Isleifson and L. Shafai, "Numerical homogenization of heterogeneous media using FVTD simulations," in *Proc. 14th Int. Symp. Antenna Technol. Appl. Electromagn. Amer. Electromagn. Conf.*, 2010, pp. 1–4.

[19] K. Sarabandi and P. Polatin, "Electromagnetic scattering from two adjacent objects," *IEEE Trans. Antennas Propag.*, vol. 42, no. 4, pp. 510–517, Apr. 1994.

Dustin Isleifson (S'01) received the B.Sc. degree in electrical engineering (Hons.) from the University of Manitoba, Winnipeg, MB, Canada, in 2005, where he is currently pursuing the Ph.D. degree in electrical engineering.

He conducted research in the Canadian Arctic through ArcticNet and the Circumpolar Flaw Lead System Study (CFL). He held a Canadian NSERC Canada Graduate Scholarship CGS-M in 2006 and currently holds an NSERC Canada Graduate Scholarship CGS-D3. His current research interests are in the areas of microwave remote sensing, computational electromagnetics, and arctic science.

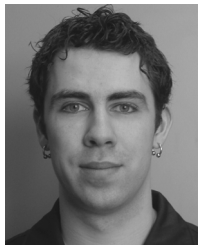

Ian Jeffrey (M'11) received the B.S. degree in computer engineering (Hons.), and the M.S. and Ph.D. degrees in electrical and computer engineering from the University of Manitoba, Winnipeg, MB, Canada, in 2002, 2004, and 2011, respectively.

In 2008, he was an Intern at Cadence Design Systems, Inc., Tempe, AZ, where he worked with the Department of Custom Integrated Circuits Advanced Research and Development. He currently holds a MITACS industrial postdoctoral fellowship with the National Research Council Canada's Institute for Biodiagnostics (NRC-IBD). His current research interests include finite-volume and discontinuous galerkin time-domain methods, fast algorithms for computational electromagnetics, high-performance computing, and inverse problems.

Lotfollah Shafai (LF'07) received the B.Sc. degree in electrical engineering from the University of Tehran, Tehran, Iran, in 1963 and the M.Sc. and Ph.D. degrees in electrical engineering from the Faculty of Applied Sciences and Engineering, University of Toronto, Toronto, ON, Canada, in 1966 and 1969, respectively.

In 1969, he joined the Department of Electrical and Computer Engineering, University of Manitoba as a Sessional Lecturer, and became Assistant Professor in 1970, Associate Professor in 1973, and Professor in 1979. Since 1975, he has made special effort to link the university research to the industrial development by assisting industries in the development of new products or establishing new technologies. To enhance the University of Manitoba contact with industry, in 1985 he assisted in establishing "The Institute for Technology Development," and was its Director until 1987, when he became the Head of the Electrical Engineering Department. His assistance to industry was instrumental in establishing an Industrial Research Chair in Applied Electromagnetics at the University of Manitoba in 1989, which he held until 1994. He has been a participant in nearly all Antennas and Propagation symposia and participates in the review committees. In 1986, he established the symposium on Antenna Technology and Applied Electromagnetics (ANTEM) at the University of Manitoba that is currently held every two years.

Dr. Shafai has been the recipient of numerous awards. In 1978, his contribution to the design of a small ground station for the Hermus satellite was selected as the 3rd Meritorious Industrial Design. In 1984, he received the Professional Engineers Merit Award and in 1985, "The Thinker" Award from Canadian Patents and Development Corporation. From the University of Manitoba, he received the "Research Awards" in 1983, 1987, and 1989; the Outreach Award in 1987; and the Sigma Xi, Senior Scientist Award in 1989. In 1990, he received the Maxwell Premium Award from the Institute of Electrical Engineers (London) and in 1993 and 1994, the Distinguished Achievement Awards from the Corporate Higher Education Forum. In 1998, he received the Winnipeg RH Institute Foundation Medal for Excellence in Research. In 1999 and 2000, he received the University of Manitoba, Faculty Association Research Award. He was elected a Fellow of The Royal Society of Canada in 1998. He was a recipient of the IEEE Third Millennium Medal in 2000 and in 2002, was elected a Fellow of The Canadian Academy of Engineering and Distinguished Professor at The University of Manitoba. In 2003, he received an IEEE Canada "Reginald A. Fessenden Medal" for "Outstanding Contributions to Telecommunications and Satellite Communications" and a Natural Sciences and Engineering Research Council (NSERC) Synergy Award for the "Development of Advanced Satellite and Wireless Antennas." He holds a Canada Research Chair in Ap-

plied Electromagnetics and was the International Chair of Commission B of the International Union of Radio Science (URSI) for 2005-2008. In 2009, he was elected a Fellow of the Engineering Institute of Canada, and was the recipient of an IEEE Chen-To-Tai Distinguished Educator Award. In 2011, he received a Killam Prize in Engineering from The Canada Council for the Arts, for his "outstanding Canadian career achievements in engineering, and his work in antenna research." He is a member of URSI Commission B and was its chairman during 1985-1988.

Joe Lovetri (SM'09) received the B.Sc. (Hons.) and M.Sc. degrees in electrical engineering from the University of Manitoba, Winnipeg, MB, Canada, in 1984 and 1987, the Ph.D. degree in electrical engineering from the University of Ottawa, Ottawa, ON, in 1991, and the M.A. in philosophy from the University of Manitoba in 2006.

From 1984 to 1986, he was an EMI/EMC Engineer at Sperry Defence Division, Winnipeg, MB, Canada, and from 1986 to 1988, he held the position of TEMPEST Engineer at the Communications Security Establishment, Ottawa. From 1988 to 1991, he was a Research Officer at the Institute for Information Technology of the National Research Council of Canada. His academic career began in 1991 when he joined the Department of Electrical and Computer Engineering, The University of Western Ontario, London, where he remained until 1999. In 1997–1998, he spent a sabbatical year at the TNO Physics and Electronics Laboratory, The Netherlands, conducting research in time-domain computational methods and ground penetrating radar. In 1999, he joined the University of Manitoba, where he is currently a Professor in the Department of Electrical and Computer Engineering. From 2004 to 2009, he was the Associate Dean (Research and Graduate Programs) for the Faculty of Engineering. His main research interests lie in the areas of time-domain computational electromagnetics, modeling of electromagnetic-compatibility problems, inverse problems, and biomedical imaging.

David G. Barber received the B.Sc. and M.Sc. degrees from the University of Manitoba, Winnipeg, MB, Canada, in 1981 and 1987, respectively, and the Ph.D. degree from the University of Waterloo, Waterloo, ON, Canada, in 1982.

He is a Canada Research Chair (CRC) Professor of Environment and Geography and Canada Research Chair in Arctic System Science with the Clayton H. Riddell (CHR) Faculty of Environment Earth and Resources, University of Manitoba. He was appointed to a faculty position at the University of Manitoba in 1993 and received a CRC in Arctic System Science in 2002. Currently, he is Director of the Centre for Earth Observation Science and Associate Dean (Research), CHR Faculty of Environment, Earth and Resources, University of Manitoba. He has extensive experience in the examination of the Arctic marine environment as a "system," and the effect climate change has on this system. He has published many articles in the peer-reviewed literature pertaining to sea ice, climate change, and physical-biological coupling in the Arctic marine system. He led the largest International Polar Year (IPY) project in the world, known as the circumpolar flaw lead (CFL) system study. He is recognized internationally through scientific leadership in large network programs (e.g., NOW, CASES, ArcticNet, the Canadian Research Icebreaker (Amundsen), and CFL), as an invited member of several Natural Sciences and Engineering Research Council (NSERC) national committees (e.g., NSERC GSC 09; NSERC IPY, NSERC northern supplements, etc.), international committees (GEWEX, IAPP, CNC-SCOR, IARC, etc.), and invitations to national and international science meetings (e.g., American Geophysical Union (AGU), Canadian Meteorological and Oceanographic Society (CMOS), American Meteorological Society (AMS), American Society for Limnology and Oceanography (Spain), IMPACTS (Russia), European Space Agency (ESA, Italy), Arctic Frontiers (Norway), etc). He currently supervises nine M.Sc. students; nine Ph.D. students, four postdoctoral fellows, and nine full-time research staff.